Volume 1 | Number 1 | Jan 2013 | Pages 1–100

Dalton Transactions

An international journal of inorganic chemistry
www.rsc.org/dalton

ROYAL SOCIETY OF CHEMISTRY

ROYAL SOCIETY OF CHEMISTRY

www.rsc.org/dalton

Water-Assisted Proton Delivery and Removal in Bio-inspired Hydrogen Production Catalysts

Ming-Hsun Ho, Molly O'Hagan, Michel Dupuis, Daniel L. DuBois, R. Morris Bullock, Wendy Shaw*, and Simone Raugei*

Center for Molecular Electrocatalysis, Pacific Northwest National Laboratory, P.O. Box 999, K2-57, Richland, WA 99352

wendy.shaw@pnnl.gov; simone.raugei@pnnl.gov

Abstract

Electrocatalysts for H_2 production are envisioned to play an important role in renewable energy utilization systems. Nickel-based catalysts featuring pendant amines functioning as proton relays in the second coordination sphere of the metal center have led to catalysts achieving turnover frequencies as high as 10^7 s^{-1} for H_2 production. The fastest rates are observed when water is present in solution, with rates up to 10^3 times faster than those found in dry solvent. The focus of this paper is to provide mechanistic insight into the unexpected enhancement due to water. Addition of H_2 to $[Ni(P^R_2N^{R'}_2)_2]^{2+}$ was previously shown to give three isomers of a Ni(0) product with two protonated amines, where the N-H can be endo or exo to the Ni. By investigating the deprotonation of two N-protonated Ni(0) intermediates resulting from the addition of H_2 to $[Ni(P^R_2N^{R'}_2)_2]^{2+}$, we observe by NMR spectroscopy studies an enhancement in the rate of deprotonation for protons positioned on the pendant amine next to the metal (endo) vs. protons that are positioned away from the metal (exo). Computational studies suggest that for smaller bases, desolvation energy of the of the exogenous base is the primary contribution limiting the rate of endo deprotonation, while steric accessibility and facile proton movement also contribute. For more bulky bases, steric accessibility can play the dominant role. The significant reduction in these barriers observed in the presence of water has important implications for disfavoring less productive catalytic pathways and increasing catalytic rates.

Introduction

The increased use of electrical energy from intermittent renewable energy sources would be facilitated by the ability to efficiently store the energy produced as chemical energy (fuels) and retrieve it on demand.[1,2] Electrocatalysis will have a prominent role in such energy conversions. One of the candidates as an energy storage vector is molecular H_2, with storage and utilization of energy being achieved by H_2 production and oxidation. Significant efforts have been made to design molecular complexes that employ abundant metals[3–7] such as nickel,[8–10] cobalt[3,11] and iron[12–15] as electrocatalysts for the production or oxidation of H_2.

Our laboratory has developed Ni- and Fe-based electrocatalytic platforms that contain pendant amines in the second coordination sphere of the metal center,[9] as shown in Scheme 1 for $[Ni(P^R_2N^{R'}_2)_2]^{2+}$. The pendant amines have been shown to perform several key roles, facilitating the heterolytic H-H bond cleavage and formation,[16] intramolecular proton transfer,[17] and intermolecular delivery of protons to the metal complex from an external proton source (H_2 production) or from the catalysts to an exogenous base (H_2 oxidation).[18]

The proposed catalytic cycle for H_2 oxidation and production by $[Ni(P^R_2N^{R'}_2)_2]^{2+}$ complexes shown in Scheme 1 is supported by extensive experimental and theoretical investigations.[16,18–28] Oxidation of H_2, depicted with the counterclockwise blue arrow in Scheme 1, is proposed to proceed through the formation of a transient H_2 adduct that promptly undergoes heterolytic H_2 splitting with the formation of an N-protonated nickel hydride species (abbreviated as **eNiH^{2+}**). This complex quickly evolves to the experimentally observed doubly-protonated Ni(0) species (abbreviated as **ee^{2+}**), where the two N-H bonds are oriented endo with respect to the metal center.[†] Two proton and two electron transfers (that could involve proton-coupled electron transfers)[29–31] complete the catalytic cycle.[16] We previously identified deprotonation as a possible rate-determining step under some experimental conditions in the catalytic oxidation of H_2, due to the inaccessibility of the endo site to the external base, especially when bulky bases are used.[25]

H_2 production follows the clockwise red arrow in the cycle, with successive reduction and protonation steps. For the protonation steps, previous studies on $[Ni(P^{Cy}_2N^{Bn}_2H)_2]^{2+}$ (Cy =

[†] Throughout this paper, **e** is used to denote protonation *endo* to the metal, **x** is used to denote protonation *exo* to the metal center, and **NiH** denotes protonation at the metal center to make the nickel hydride. Overall charges are as indicated.

cyclohexyl, Bn = benzyl) have revealed that branching of the cycle occurs because protonation can lead to a less productive isomer.[18] Along with the doubly protonated ee^{2+} intermediate resulting from two protonations of the reduced Ni(I) complex, two other species are also observed: the endo/exo, ex^{2+}, and exo/exo, xx^{2+}, isomers (Scheme 1).[32,33] Similar species have been observed for Fe-based complexes.[33,34] The three isomers differ in the orientation of the N-H bonds; all three are observed in solution and are of similar energies. Isomer ee^{2+} has both N-H bonds endo to the nickel, while isomer xx^{2+} has both N-H bonds exo to the nickel, in a "pinched" (N-H-N) configuration. Isomer ex^{2+} has a mixed endo-exo geometry. The exo protonation site has been shown to be kinetically preferred due to the steric inaccessibility of the endo site.[18] Recovery of catalytic activity requires isomerization between these species because only the ee^{2+} isomer is catalytically competent. This isomerization process has been studied in detail by experimental and computational methods,[18] and is regulated by a combination of steric effects, hydrogen bonding, and electrostatic interactions. Importantly, it has been shown that when using weak or bulky bases, barriers for intermolecular protonation/deprotonation are significantly higher than those for any intramolecular proton transfers involved in the catalytic cycle. The detrimental role of exo protonation on catalytic rates has been discussed previously,[16,18,21,35] and this information has been exploited to design catalysts with exceedingly high rates for H_2 production.[20,21,24,36]
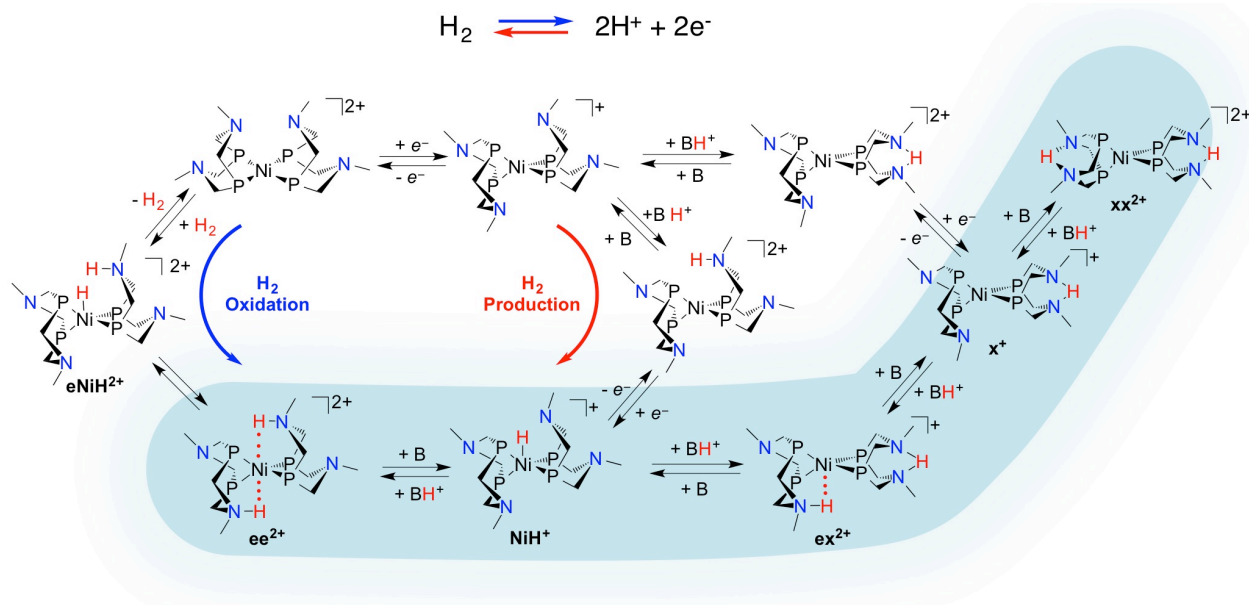
Scheme 1. Proposed catalytic mechanism of oxidation/production of hydrogen by $[Ni(P^R_2N^{R'}_2)_2]^{2+}$. The part of the catalytic cycle investigated in the present study is highlighted with the cyan ribbon. The substituents on phosphorus (cyclohexyl) and nitrogen (benzyl) are not shown for clarity.

Water has been shown to accelerate the rate of H_2 production by $[Ni(P^R_2N^{R'}_2)_2]^{2+}$ electrocatalysts.[26,27] Turnover frequency (TOF) increases up to 10^3 fold have been observed in acetonitrile/water solutions and up to 10^4 in protic ionic liquids/water solutions.[24,26,36,37] This observation suggests that water facilitates proton delivery to the catalyst and/or the interconversion of the doubly protonated isomers, and both have been proposed to influence the observed catalytic rates. In this paper, we investigate the role of water on the interconversion between the doubly protonated $\mathbf{ee^{2+}}$, $\mathbf{ex^{2+}}$ and $\mathbf{xx^{2+}}$ isomers (Scheme 1, cyan ribbon). Using NMR spectroscopy and quantum chemical calculations, we analyze the possible mechanisms by which water facilitates proton delivery to and from the catalysts. Factors that contribute to the rate enhancements are discussed, including desolvation, proton transfer, and steric accessibility.

Results

Kinetics study from 2D-NMR spectroscopy experiments

The effect of water on the isomerization process was investigated using the well-studied $[Ni(P^{Cy}_2N^{Bn}_2)_2]^{2+}$ catalyst for H_2 oxidation[17,18,38] as a model system for the doubly protonated intermediates that are not observable in hydrogen production catalysts due to their short lifetimes relative to the timescale of the NMR experiments.

In the conditions tested in the present study (addition of aniline and aniline/water mixtures), the isomer distribution obtained from the NMR spectroscopy measurements shows that changing the amount of water and aniline has a negligible effect on the ratio of isomers observed at equilibrium, with the exception of the formation of a small amount of the Ni hydride complex $[HNi(P^{Cy}_2N^{Bn}_2)_2]^+$, the concentration of which remains smaller than 4% (Figure 2). According to the observed distribution, free energy differences among isomers are within 1 kcal/mol. Calculations carried out on doubly protonated isomers of $[Ni(P^{Cy}_2N^{Me}_2)_2]^{2+}$ substantiate the experimental observation (Table S1). All of the calculations presented in this paper were carried out on $[Ni(P^{Cy}_2N^{Me}_2)_2H_x]^{x+}$ (x = 1 or 2) complexes, where the benzyl substituents used in the experimental studies are replaced by methyl groups that reduce the computational cost. This choice is validated by previous theoretical and experimental

investigations.[17,18] Changes in the relative free energies of isomers are less than 0.5 kcal/mol in pure acetonitrile compared to pure water solutions (Table S1).
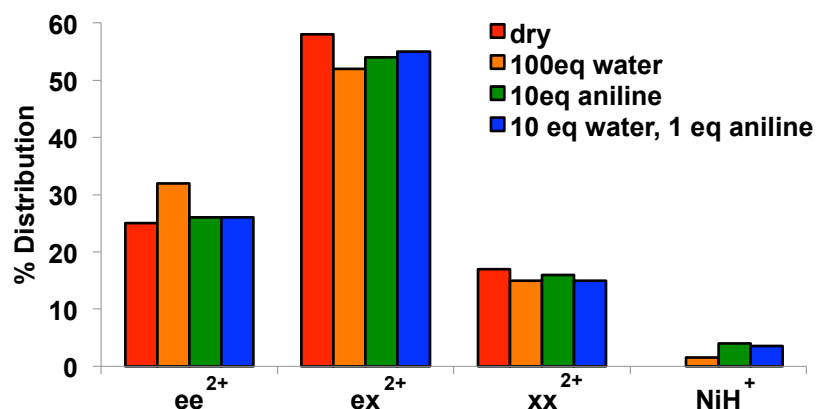
Figure 2. Equilibrium distribution of doubly protonated isomers in CD_3CN, 10 mM $[Ni(P^{Cy}_2N^{Bn}_2H)_2]^{2+}$ at 25 °C, with different additives.

Although water does not change the relative distribution of the doubly protonated isomers, the concentration of the **NiH$^+$** species in the presence of aniline increases when water is added. This might be due to the increased basicity of aniline in the presence of water. Indeed, consistent with experimental observations, the calculations discussed below show that hydrogen bonding of water to anilinium in acetonitrile increases the pK_a of the anilinium from 10.6 to 11.9. The higher basicity of aniline favors deprotonation and, therefore, the formation of the **NiH$^+$** intermediate. This increased basicity will also facilitate faster isomerization rates, as observed above.

The interconversion of the kinetically preferred exo protonation sites[18] and the catalytically competent endo sites,[16] i.e. $xx^{2+} \leftrightarrows ex^{2+} \leftrightarrows ee^{2+}$, controls the concentration of the H_2 evolution intermediate **ee^{2+},** and therefore may represent the bottleneck in catalysis (Scheme 1). As reported previously, in the case of the $[Ni(P^{Cy}_2N^{Bn}_2)_2]^{2+}$ complex, this isomerization process occurs over a period of days under rigorously dry conditions.[18] The effect of water on this isomerization process in the presence and absence of base was determined by monitoring the time required for the **ee^{2+}**, **ex^{2+}**, and **xx^{2+}** isomers to reach equilibrium using $^{31}P\{^1H\}$ NMR spectroscopy. As reported previously,[18] the **ee^{2+}** isomer, which can be generated by the addition of H_2 to $[Ni(P^{Cy}_2N^{Bn}_2)_2]^{2+}$, isomerizes to an equilibrium distribution of **ee^{2+}**, **ex^{2+}** and **xx^{2+}** by a stepwise intermolecular proton transfers of one proton from the interior endo site to the exterior exo site, as shown in Scheme 1. The rate-determining step in this equilibration process is the isomerization of the **ex^{2+}** isomer to the **xx^{2+}** isomer, which was determined to be greater than 300

times slower than the interconversion of the $\mathbf{ee^{2+}}$ and $\mathbf{ex^{2+}}$ species.[18] The primary source of this difference is in the formation of the high energy, singly protonated exo species ($\mathbf{x^{+}}$) rather than the $\mathbf{NiH^{+}}$ intermediate, as the latter was determined to be 4.6 kcal/mol more stable (see Scheme 1, cyan ribbon).[18] The time to reach equilibrium was compared by monitoring the time needed to form 50% of the equilibrium concentration of the $\mathbf{xx^{2+}}$ isomer. We previously found that the equilibration time decreases with the addition of bases, such as the conjugate bases of the acids used in catalysis, *i.e.* a 15% decrease with 10 equivalents of 2,6-dichloroaniline, and a 37% decrease with 10 equivalents of dimethylformamide (DMF).[18] Similarly, we now find that the equilibration is enhanced in the presence of water; addition of 100 equivalents of water increases the rate of isomerization by a factor of nine (Figure 1). Hydrogen bond acceptors such as ethanol, also increase isomerization by a factor of 1.6 compared to dry acetonitrile. Importantly, the most pronounced effect on isomerization rate is observed under conditions most similar to conditions that result in the maximum catalytic activity, *i.e.* with both water and base added to the solution. For instance, with the addition of 10 equivalents of aniline and 10 equivalents of water, the isomers were fully equilibrated before 1D ^{31}P NMR spectra could be acquired, *i.e.* in less than 3 minutes, which is an increase of greater than 100 times.
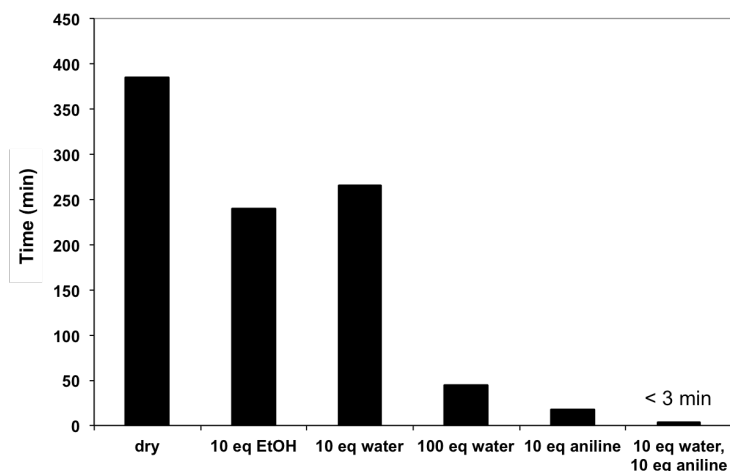
Figure 1. Comparison of the time required to form 50% of the equilibrium amount of the $\mathbf{xx^{2+}}$ isomer in CD$_3$CN, 10 mM [Ni(P$^{Cy}_2$N$^{Bn}_2$H)$_2$]$^{2+}$ at 25 ºC with different additives: ethanol, water and aniline.

Kinetics analysis

The mechanism of intermolecular exchange in the presence of water was investigated using 2D ^{31}P exchange NMR spectroscopy experiments, EXSY, to determine rate constants. As reported previously, the interconversion of the $\mathbf{ee^{2+}}$ and $\mathbf{ex^{2+}}$ isomers through $\mathbf{NiH^{+}}$ is sufficiently

rapid to be observed by EXSY spectroscopy (ms^{-1} to s^{-1} timescales; see Figures S1 and S2) in the presence of aniline; however, no exchange is observed with the **xx**$^{2+}$ isomer on the EXSY timescale under the same conditions or with the addition of water and aniline. The interconversion of the **ex**$^{2+}$ and **xx**$^{2+}$ is very slow (from seconds to hours depending on the conditions, Figure 1). Therefore this process was too slow to be determined by EXSY spectroscopy and the time to reach 50% conversion of the **xx**$^{2+}$ was used as an estimate of the isomerization rate under different conditions, discussed above. Because it is faster, the rate of interconversion of the **ee**$^{2+}$ and **ex**$^{2+}$ isomers in the presence of added water and aniline, *i.e.* conditions similar to those of electrocatalytic measurements, was obtained using EXSY spectroscopy.[39] Measurements were carried out at a constant concentration of aniline (approximately 220 mM, *i.e.* 10 equivalents per catalyst), while the concentration of water was varied from 0 to 2 M, *i.e.* 0-100 equivalents per catalyst. The rate equations derived from Scheme 2 are given below, where **B** and **BH**$^{+}$ stand for the base and its conjugate acid, respectively.

$$\frac{d[\mathbf{ee^{2+}}]}{dt} = -k_1^{(n)}[\mathbf{ee^{2+}}][\mathbf{B}][\mathrm{H_2O}]^n + k_{-1}^{(n)}[\mathbf{NiH^+}][\mathbf{BH^+}][\mathrm{H_2O}]^n = -r_1 + r_{-1}$$

$$\frac{d[\mathbf{ex^{2+}}]}{dt} = -k_2^{(n)}[\mathbf{ex^{2+}}][\mathbf{B}][\mathrm{H_2O}]^n + k_{-2}^{(n)}[\mathbf{NiH^+}][\mathbf{BH^+}][\mathrm{H_2O}]^n = -r_2 + r_{-2}$$

$$\frac{d[\mathbf{NiH^+}]}{dt} = -\frac{d[\mathbf{ee^{2+}}]}{dt} - \frac{d[\mathbf{ex^{2+}}]}{dt}$$
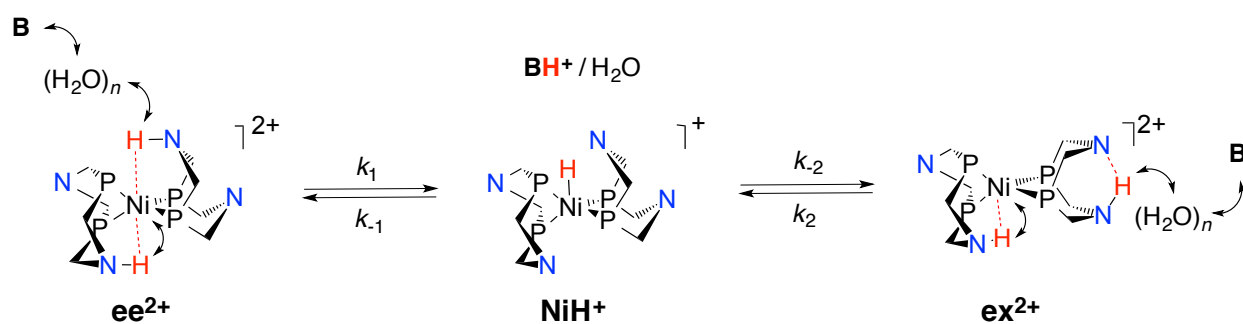
Scheme 2. Proposed mechanism of exchange between the **ee**$^{2+}$ and **ex**$^{2+}$ isomers, where $n = 0$ for k_{-2} and $n = 0$ or 1 for k_1, k_2, and k_{-1}. The substituents on the P and N atoms are not shown.

The rate of deprotonation of **ee**$^{2+}$ and the exo side of **ex**$^{2+}$ to produce the nickel hydride **NiH**$^{+}$ (r_1 and r_2, Figure 3) and the rates of reprotonation of **NiH**$^{+}$ to give **ee**$^{2+}$ and **ex**$^{2+}$ (r_{-1} and r_{-2}, Figure 4) were plotted versus the change in water concentration.

The observed deprotonation rates for both $\mathbf{ee^{2+}} \rightarrow \mathbf{NiH^+}$ and $\mathbf{ex^{2+}} \rightarrow \mathbf{NiH^+}$ have a first-order dependence ($n = 1$) on water concentration ($k_1^{(1)} = 164 \pm 6$ M^{-2} s^{-1} and $k_2^{(1)} = 151 \pm 7$ M^{-2} s^{-1}, respectively, Figure 3). The non-zero intercepts in Figure 3 for r_1 and r_2 indicate that for both processes, a significant pathway also exists that does not involve water ($n = 0$), but only aniline and the nickel complex. In agreement with our earlier report,[18] the pathway involving no water is slower for $\mathbf{ee^{2+}} \rightarrow \mathbf{NiH^+}$($k_1^{(0)} = 3.3 \pm 3$ M^{-1}s^{-1}), than for $\mathbf{ex^{2+}} \rightarrow \mathbf{NiH^+}$ ($k_2^{(0)} = 65 \pm 6$ M^{-1} s^{-1}). In contrast, in the presence of water, $k_1^{(1)}$ and $k_2^{(1)}$ are almost identical, $k_1^{(1)} = 164 \pm 6$ M^{-2} s^{-1} and $k_2^{(1)} = 151 \pm 7$ M^{-2} s^{-1}. The larger change in the deprotonation of the endo position demonstrates that water has a larger effect on the endo process, as discussed in detail below.
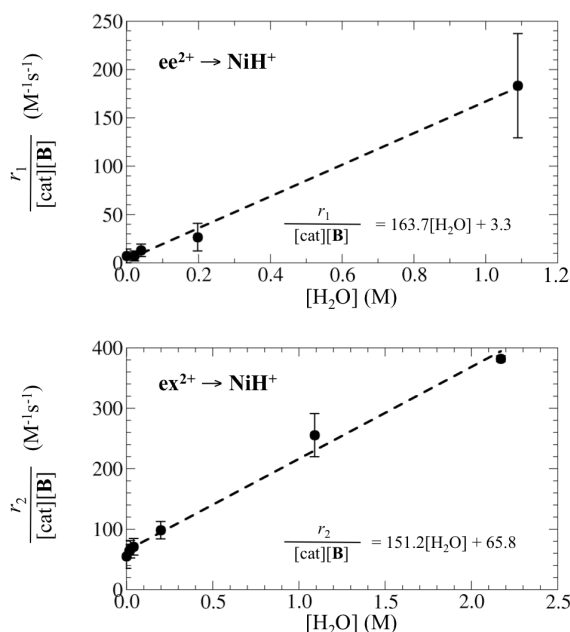
Figure 3. Rate of deprotonation of the $\mathbf{ee^{2+}}$ (r_1, top panel) and $\mathbf{ex^{2+}}$ isomers (r_2, bottom panel) to the hydride intermediate $\mathbf{NiH^+}$ versus the concentration of water, 0 to 2 M, in CD$_3$CN at 25 °C with 220 mM aniline and 22 mM [Ni(P$^{Cy}_2$N$^{Bn}_2$H)$_2$]$^{2+}$. Error bars represent one standard deviation. Rates have been normalized to the catalyst concentration ([cat]) and aniline concentration ([$\mathbf{B}$]). The dashed lines represent the linear fit to the data (equations given in the panels). In both cases the regression coefficient is $R^2 = 0.99$.

For the reprotonation reaction, the $\mathbf{NiH^+} \rightarrow \mathbf{ex^{2+}}$ step does not have an appreciable (within the experimental error) dependence on water concentration (Figure 4). In contrast, the $\mathbf{NiH^+} \rightarrow \mathbf{ee^{2+}}$ reprotonation does show a dependence on water ($k_{-1}^{(1)} = 7300 \pm 590$ M^{-2}s^{-1}). As observed for the deprotonation reactions, in both reprotonation processes, a pathway that is zero-order in water is also operative, with a rate constant of $k_{-1}^{(0)} = 2300 \pm 290$ M^{-1}s^{-1} and $k_{-2}^{(0)} =$

52000 ± 3400 M^{-1}s^{-1} for **NiH$^+$** → **ee^{2+}** and **NiH$^+$** → **ex^{2+}**, respectively. It is also worth noting that the K_{eq} obtained from the EXSY experiments is the same as that obtained in the 1D-experiments, within a 30% error.
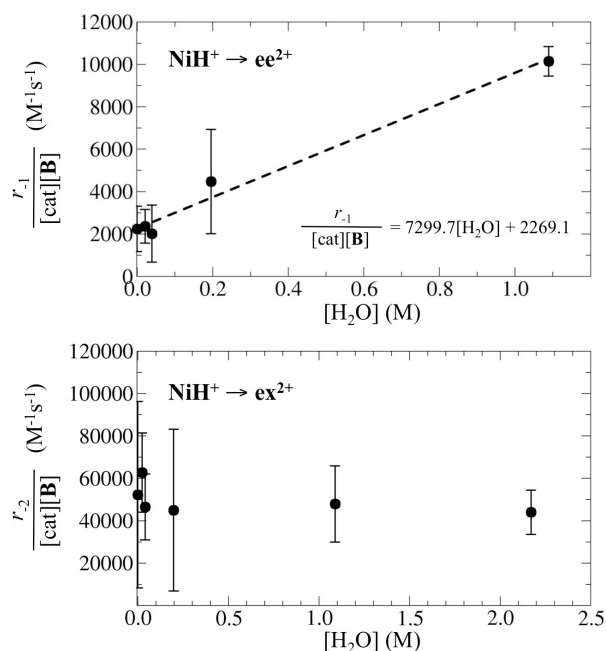
Figure 4. Rate of protonation of the **NiH$^+$** species to the **ee^{2+}** (r_{-1}, top panel) and **ex^{2+}** isomers (r_{-2}, bottom panel) versus the concentration of water, 0-2 M, in CD$_3$CN at 25 °C with 220 mM aniline and 22 mM [Ni(P$^{Cy}_2$N$^{Bn}_2$H)$_2$]$^{2+}$. Error bars represent one standard deviation. Rates have been normalized to the catalyst concentration ([cat]) and aniline concentration ([**B**]). In the top panel the dashed line represents the linear fit to the data (equation given in the panel; regression coefficient R^2 = 0.98). No appreciable dependence on water concentration is observed for the **NiH$^+$** → **ex^{2+}** process.

Computational study of the mechanism of isomerization

To understand the origin of the observed increase in the rate of isomerization due to water at both the endo and exo sites, an extensive set of quantum chemical calculations has been performed. The theoretical analysis builds on our previous investigation of the isomerization mechanism catalyzed by aniline only.[18] In the present study we have only considered the possibility of one water molecule acting as a proton shuttle from the catalysts to the base, with this model being supported by the first-order dependence on water observed experimentally in the range of concentrations examined.

The proposed mechanism of the **ee^{2+}** ⇆ **ex^{2+}** and **ex^{2+}** ⇆ **xx^{2+}** isomerization was discussed in detail previously.[18] The **ee^{2+}** ⇆ **ex^{2+}** proceeds via a Ni(II) hydride intermediate (**NiH$^+$**) as illustrated in Figures 5a and 5c. Isomerization consists of the association/dissociation

of the base and conjugate acid from the catalyst, conformational changes (chair-boat ring inversions) of the six-membered rings, and deprotonation and protonation steps. The participation of water in each of these steps is analyzed below.

We found that, in acetonitrile, deprotonation assisted by water is facilitated by a considerably reduced barrier for the proton transfer from the protonated pendant amine to an external base and the subsequent dissociation of the conjugated acid, which outbalance desolvation penalties not present in dry solution. In the following we will focus the discussion on the deprotonation steps (last two steps in the free energy profiles of Figure 5). An analysis of the other steps that complete the reaction mechanism is given in the Supporting Information.

Isomerization is initiated by the formation of binary association complexes between the catalysts and base, or ternary association complexes between the catalyst, water and base. As discussed in the Supporting Information, the formation of a ternary complex, where water bridges the catalyst and the base (Figures 5b and 5d, step 3), is unfavorable because of the loss of solvation energy of the each individual species, and in particular of water, which is not counterbalanced by the formation of hydrogen bonds between the three species. Despite this penalty, proton transfer mediated by water is more favorable than direct proton transfer between the catalyst and aniline. The free energy for the proton transfer from the endo position in ee^{2+} to the base is 2.7 kcal/mol (Figures 5b, step 4) when water mediates the transfer and 6.0 kcal/mol in dry solution (Figures 5a, step 3). In addition, the free energy barrier to dissociate anilinium from the ternary complex (2.4 kcal/mol, Figures 5b and 5d, step 5) is also smaller than the corresponding value for the binary complex (6.9 kcal/mol, Figure 5a, step 4). The cumulative barrier for the two steps (proton transfer to aniline and subsequent dissociation of anilinium) at the endo position is 13.1 kcal/mol in dry solvent but is only 5.1 kcal/mol in the presence of water. The calculated overall barrier for deprotonating ee^{2+} is reduced from 21.2 kcal/mol when water does not participate in the deprotonation to 18.4 kcal/mol when water shuttles the proton from the pendant amine to aniline. Deprotonation at the exo position in ex^{2+} shows similar energetic features. The cumulative barrier for the proton transfer to aniline in the association complex and the final dissociation is the complex of 12.9 kcal/mol (Figure 5c, steps 3 and 4) in dry conditions and 5.4 kcal/mol when deprotonation is mediated by water (Figure 5d, steps 4 and 5). The total barrier for deprotonating the exo position is 21.6 kcal/mol and 19.0 kcal/mol in dry solution and water, respectively.

10
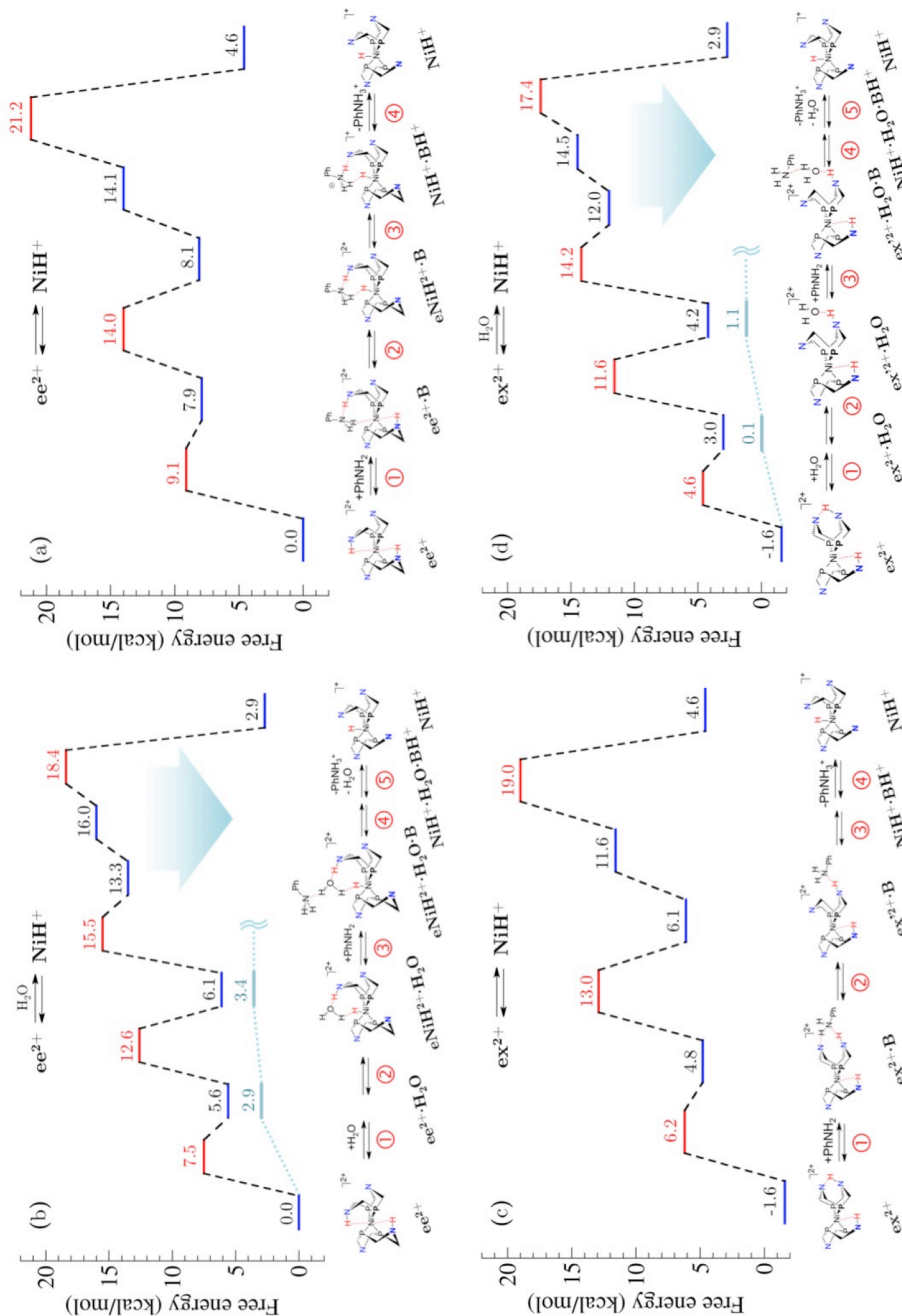
Figure 5. Standard state free energy diagram for the **ee²⁺ ⇆ NiH⁺** and **ex²⁺ ⇆ NiH⁺** isomerization mechanisms in the presence of aniline, **B**, *in dry acetonitrile* (a and c), and *in the presence of water* (b and d). The relative free energies with respect to **ee²⁺ + B** (a and c) or to **ee²⁺ + H₂O + B** (b and d) of the various intermediates (blue) and the transition states (red) are indicated. The R and R′ groups are not shown. In panels b and d, the free energy for addition of a molecule of water to **ee²⁺** in aqueous solution (described as a polarizable continuum) is also given in light blue. The blue arrow is intended to indicate the lower energy of the proton transfer from the catalysts to water as a consequence of the reduced energetics for the formation of the association complex. The elementary steps are sequentially numbered in the equations provided at the bottom of each panel. For clarity, some of the species in the chemical equations are not shown: **ee²⁺·H₂O**, **ex²⁺·H₂O** and **NiH⁺·H₂O·BH⁺** (with BH⁺ bound to the exo site) in panels b and d, steps 1 and 4; **NiH⁺·BH⁺** (with BH⁺ bound to the exo site) in step 3, panel c. [The caption will be printed sideways full page]

11

To understand the origin of the lower barrier in the presence of water, we decomposed the reaction free energy in its electronic, thermal and solvation contributions (Table S2).[18] This decomposition shows that the lower energy cost for proton transfer is primarily due to the stabilization of the protonated anilinium, reflecting better solvation when it is associated with water and the complex, rather than with the complex alone. Indeed, in the binary complex, anilinium is closer to the catalyst pocket and less exposed to the solvent (Figure 6), which results in a less favorable solvation free energy change for the **eNiH^{2+}·B → NiH$^+$·BH$^+$** proton transfer (Figure 5a, step 3, $\Delta G°_{sol}$ = +9.3 kcal/mol) than for **eNiH^{2+}·H$_2$O·B → NiH$^+$·H$_2$O·BH$^+$** proton transfer (Figure 5b, step 4, $\Delta G°_{sol}$ = +3.7 kcal/mol). The corresponding values for the proton transfer at the exo position are $\Delta G°_{sol}$ = +8.6 kcal/mol for **ex'$^{2+}$·B → NiH$^+$·BH$^+$** (where the prime indicates the exo pronated amine is not engaged in *intra*molecular hydrogen bonding, see Figure 5c), and $\Delta G°_{sol}$ = +2.3 kcal/mol for **ex'$^{2+}$·H$_2$O·B → NiH$^+$·H$_2$O·BH$^+$**. The larger influence on the **ee^{2+}** isomer is consistent with the greater enhancement in the presence of water observed experimentally.
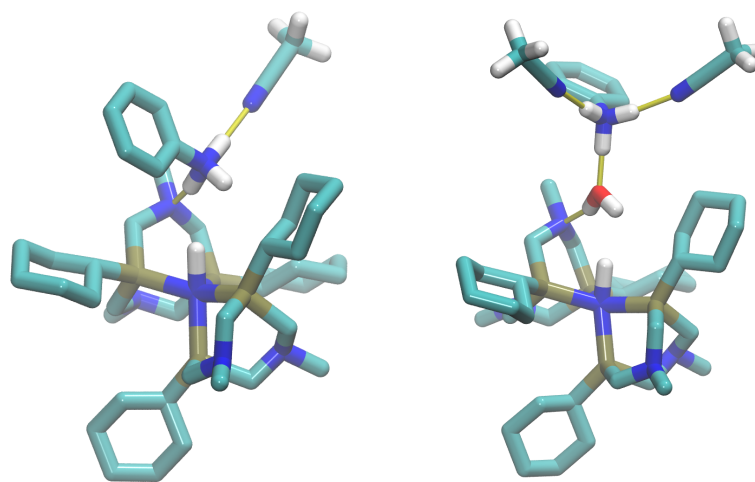
Figure 6. Structure of the **NiH$^+$·BH$^+$** (left) and **NiH$^+$·H$_2$O·BH$^+$** (right) association complexes. For clarity, the non-polar hydrogen atoms of the hydride intermediate are not shown. Hydrogen bonds are shown as yellow sticks.

The lower activation barrier for dissociating anilinium from the ternary complex can be explained in terms of a weaker hydrogen bond between water and anilinium than between the pendant amine and anilinium, due to much larger difference in pK_a between anilinium (pK_a = 10.6)[39] and hydronium (pK_a = 1.5 as calculated in the present study) than between anilinium and the endo protonated pendant amine (pK_a = 13.5).[16,22] Indeed, a natural bond orbital (NBO) analysis of **NiH$^+$·H$_2$O·BH$^+$** and **NiH$^+$·BH$^+$** indicates a significantly smaller charge transfer from

one lone pair of the water oxygen, lp(O), to the antibonding σ*(N−H) orbital than from the lone pair on the pendant amine, lp(N). According to the NBO second-order perturbation framework,[40] the magnitude of the lp(O)→σ*(N−H) and lp(N)→σ*(N−H) charge transfer due to hydrogen bond interactions have been estimated to be 37 kcal/mol and 325 kcal/mol, respectively. Note that these energies are not a measure of the hydrogen bond energy but just an estimate of the charge transfer from the O and N lone pairs to the antibonding N-H σ orbital.

Quantum chemical calculations have shown that, in qualitative agreement with previous observations,[41] anilinium preferentially hydrogen bonds to water in acetonitrile/water solution. In contrast, in the case of aniline, binding to acetonitrile is slightly favored over water. Consequently, the basicity of aniline in acetonitrile is higher when water is present. The pK_a of anilinium depends on the number of water molecules hydrogen bonded to it. The calculated value increases from 10.6 kcal/mol in dry acetonitrile to 11.4 kcal/mol, 12.0 kcal/mol and 12.9 kcal/mol in the presence of one, two and three hydrogen bonded water molecules, respectively. The higher basicity of aniline in the presence of water makes the deprotonation of **ee^{2+}** and **ex^{2+}** less endothermic. The calculated barrier for the endo protonation of the **NiH$^+$** intermediate is 1.1 kcal/mol lower in the presence of water, while the barrier for the exo protonation is within 0.2 kcal/mol.

It is of interest to analyze the energetics for the association of water is in a purely aqueous environment (described here as a continuum). The results presented above suggest that in water solutions, solvation/desolvation steps reported in Figure 5b and 5d (steps 1, 2 and 3) should be more facile because water is the solvent and, at the same time, the deprotonating agent. The calculations in pure water reported in Figure 5b and 5d fully support this prediction (blue lines). As can be seen, addition of water is less endothermic (step 1) and, most important, the desolvation penalty, which in acetonitrile solution characterizes the formation of the ternary complex between the catalysts, water and aniline, is clearly not present in aqueous solutions (pictorially indicated with two wavy lines in Figure 5). As we shall discuss in the next section, this result has profound implications for the electrocatalytic H$_2$ production in aqueous solutions.

Discussion

Water has been shown to accelerate the rate of H_2 production by $[Ni(P^R_2N^{R'}_2)_2]^{2+}$ electrocatalysts.[26,27] In recent investigations, it has been found that proton delivery to the catalysts (for H_2 production) is a bottleneck for catalysis in dry solvent.[18] This bottleneck is caused by the interconversion of the kinetically[18,42] and sometimes thermodynamically favored,[32] **ex²⁺** and **xx²⁺** isomers to the **ee²⁺** isomer, which features protonated pendant amines with protons properly positioned for H_2 formation. In catalysts for H_2 oxidation, a shift in the potential of the catalytic wave is observed when water is added to the catalytic reaction in the presence of a bulky, strong base.[25] This suggests that the mechanism shifts from an initial oxidation followed by a proton transfer, to one in which the deprotonation occurs first, facilitated by the presence of water. These observations suggest that water facilitates proton movement by directing protons to the right position and/or reducing protonation/deprotonation barriers.

We analyzed the role of water in proton delivery and removal by studying the mechanism of isomerization that transfers the proton from the endo position to the exo position, i.e. the **ee²⁺** to **ex²⁺** and **xx²⁺** species for the $Ni(P^{Cy}_2N^{R'}_2)_2]^{2+}$ electrocatalysts for H_2 oxidation using aniline as a base (where R´ = Bn for experimental studies and R´ = Me for computational studies). These complexes are used as a model for H_2 production catalysts whose doubly protonated intermediates are not observable by NMR due to their short lifetimes relative to the timescale of the NMR experiments. The interconversion rates will be faster with the less basic pendant amines and the driving force typical of H_2 production for the H_2 production catalysts; however, the species, isomerization processes, and trends observed with varying conditions are expected to be, and under some conditions shown to be, similar in the reverse direction.[42] As previously reported with base only, the addition of water and base facilitates isomerization but does not significantly alter the distribution of isomers. In these studies, we find that water further enhances the rate of isomerization with respect to base alone. The addition of 10 equivalents of water and 10 equivalents of aniline resulted in a 128-fold acceleration of the equilibration rate. However, as found in the presence of base alone, the **ex²⁺** ⇆ **xx²⁺** isomerization still occurs on the timescale of seconds to minutes. The **ee²⁺** ⇆ **ex²⁺** isomerization is at least 100-fold faster, occurring on the order of milliseconds, and can be observed by EXSY NMR spectroscopy, allowing a detailed kinetic analysis. The deprotonation of both **ee²⁺** and **ex²⁺** proceed through a common Ni hydride intermediate, **NiH⁺**, with a similar observed rate constant ($k_1 = 164 \pm 6$ M⁻²

14

s^{-1} and $k_2 = 151 \pm 7$ M^{-2} s^{-1}, respectively, Figure 3). Two isomerization pathways are operative: a fast pathway that involves water (first order in water) and a slow pathway that is independent of water concentration. The calculated barriers for the *endo* reprotonation of the nickel hydride (**NiH$^+$**) are consistent with experimental data. In agreement with a previous report,[18] the pathway involving no water for the endo deprotonation is slower (rate constant 3 ± 3 M^{-1} s^{-1}) than the pathway involving no water for the exo deprotonation (rate constant 65 ± 6 M^{-1} s^{-1}). Therefore, water has a larger effect on the deprotonation of the endo positioned amine.

Our detailed computational analysis surprisingly showed that desolvation energy, not steric congestion, dominates the role of water in deprotonation. The reduced steric penalty for water associating with the endo positioned amine (**ee^{2+}·H$_2$O** complex) compared to the endo positioned amine with base only (**ee^{2+}·B**) is overwhelmed by a greater loss of solvation energy associated with the formation of the **eNiH^{2+}·H$_2$O·B** ternary complex.

The present computational study further suggests that water facilitates deprotonation by shuttling the proton between the catalyst and the base. In the presence of water, deprotonation begins with the association of the complex with water and the base. Although the formation of the ternary association complex is disfavored with respect to the binary association complex (*i.e.* without water), deprotonation mediated by water is favored over deprotonation in dry acetonitrile. Indeed, in the ternary complex, the base is more exposed to the solvent, and proton transfer with the formation of the conjugate acid (anilinium) is driven by more favorable solvation energy. This favorable solvation contribution alone amounts to about 5 kcal/mol (Table S2), with small differences observed between the endo and exo protonation sites. In addition, we have found that dissociation of anilinium from the ternary complex (**NiH$^+$·H$_2$O·BH$^+$**) is easier than from the binary complex (**NiH$^+$·BH$^+$**) as a result of a weaker hydrogen bond between anilinium and water than between anilinium and the hydride **NiH$^+$**.

While desolvation was the primary effect of water with anilinium, sterics may play a dominant role if larger bases are used. To test this hypothesis, additional calculations were performed with triethylamine (Et$_3$N), a base commonly used for H$_2$ oxidation catalysis. Et$_3$N is a bulkier and stronger base than aniline (the pK_a of the conjugate acid of Et$_3$N is 18.8)[39]. Because of its large size, a boat-to-chair inversion of the endo-protonated six-membered ring is required to allow binding of Et$_3$N to the endo site (Figure 7). This inversion does not occur when Et$_3$N binds to **e/NiH^{2+}·H$_2$O.** Overall, for Et$_3$N the formation of **e/NiH^{2+}·B** and **e/NiH^{2+}·H$_2$O·B** are

endothermic by 15.0 kcal/mol and 11.9 kcal/mol, respectively. The ternary complex is more stable than the binary complex by about 3 kcal/mol, while the reverse is true for aniline. Therefore, in the case of very bulky bases, the presence of water may provide the additional benefit of a reduced steric penalty associated with the binding of water to the endo position rather than the base itself, as suggested previously based on experimental observations.[25]
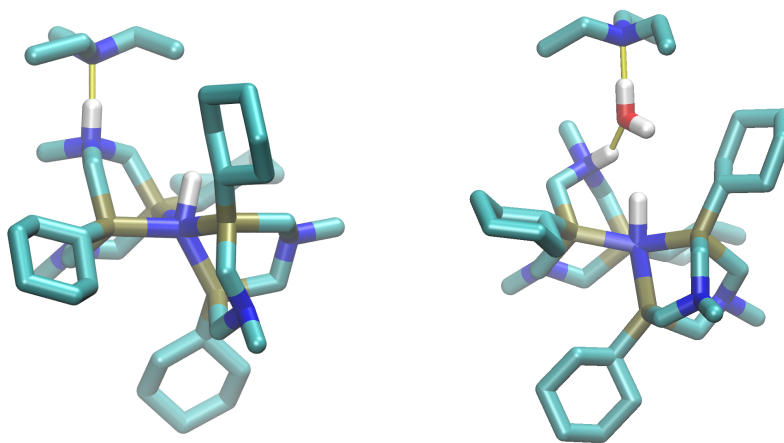
Figure 7. Binding of triethylamine, Et$_3$N. Structure of the **eNiH^{2+}·Et$_3$N** (left) and **eNiH^{2+}·H$_2$O·Et$_3$N** (right) association complexes. For clarity, the non-polar hydrogen atoms are not shown. Hydrogen bonds are shown as yellow sticks.

A key conclusion from this study is that in aqueous environments, kinetic bottlenecks associated with protonation/deprotonation events will be considerably reduced. The calculated barrier for the proton transfer between the protonated pendant amine and a base assisted by water is far smaller than the barrier for direct transfer (about 5 kcal/mol and 13 kcal/mol, respectively, see Figure 5b and 5d, steps 4 and 5). We have also shown that in an aqueous environment the solvation/desolvation steps reported in Figure 5b and 5d (steps 1, 2 and 3) are more facile because water is the solvent and the deprotonating agent (cyan lines in Figure 5b and 5d). Without the kinetic bottleneck for deprotonation and, conversely, protonation (schematically indicated with a down arrow in Figure 5b and 5d), the concentration of the **ee^{2+}** isomer would become dependent on the *thermodynamic* distribution of the species, not the *kinetics* of the isomerization process.

For [Ni(P$^{Cy}_2$N$^{R'}_2$)$_2$]$^{2+}$ catalysts, the shift in steady state concentrations from the kinetic distribution, which is almost exclusively exo protonation,[18] to the thermodynamic distribution, which includes the **ee^{2+}** isomer,[16,18,25,32] could explain the resulting increase in the catalytic H$_2$ production rates. For the [Ni(P$^{Ph}_2$N$^R_2$)]$^{2+}$ family of H$_2$ production catalysts, the thermodynamic

distribution of isomers, as well as the TOFs observed, are both substantially influenced by the basicity of the pendant amine. Therefore, if the kinetic bias for the protonation site is removed by water, similar rates are expected among catalysts that contain pendant amines with similar basicity. Consistent with this hypothesis, in media with high water content, observed TOFs are much higher than those observed at low water concentrations. For example, the maximum catalytic TOF reported for $[Ni(P^{Ph}_2N^{C_6H_4OH}_2)_2]^{2+}$ is 1.7×10^5 s^{-1} in acetonitrile solution with 0.9 mole fraction water, while it is only 35 s^{-1} in dry acetontrile.[37] The TOF for this complex is similar in magnitude to the TOFs for other catalysts in the $[Ni(P^{Ph}_2N^{C_6H_4X}_2)_2]^{2+}$ series in protic ionic liquids media with 0.7 mole fraction water (X = Br, TOF = 1×10^6 s^{-1}; X = OMe, 4×10^5 s^{-1} and X = H, 5×10^5 s^{-1}).[36] These rates are 2-3 orders of magnitude faster than those observed for this series of catalysts in dry acetonitrile conditions.

Conclusions

Experimental and computational studies probed the role of water on the H$_2$ oxidation catalysts $[Ni(P^{Cy}_2N^{R'}_2)_2]^{2+}$. Experimental data suggest water enhances protonation/deprotonation for endo positioned protons and deprotonation of exo positioned protons, with a greater enhancement from the endo position. Computational analysis suggests that this is mostly due to the desolvation energy required to bring the base to the complex, but also includes contributions from enhanced steric access and the ease of proton transfer. The facile movement of protons in the presence of water has significant implications for catalysis with these complexes, avoiding a less productive isomer that is kinetically preferred, and achieving the thermodynamic distribution of isomers that has a much higher percentage of the active isomer. The significance of water on these catalysts goes beyond simple solvation and is under further investigation in our laboratory. In light of this evidence, current efforts in our center focus on the design of water-soluble catalysts.

Experimental Section

Materials. All samples and solutions were prepared under a nitrogen atmosphere. An Innovative Technologies Pure Solv™ solvent purification system was used for solvent purification unless otherwise noted. CD$_3$CN was purified by distillation from P$_2$O$_5$. Aniline was dried with KOH and purified by distillation. Ultra high purity (99.999%) hydrogen was used after being dried by passage through an in-line drier (OxypurgeN) in series with an AT

indicating cartridge (Alltech).   Water was purified by a MillQ system and deoxygenated by sparging with a nitrogen steam.

Synthesis of Ni complexes. Previously reported procedures were followed for the synthesis of $[Ni(P^{Cy}_2N^{Bn}_2)_2][BF_4]_2$.[17,32]

NMR Spectroscopy Sample Preparation. All samples and solutions were prepared under a nitrogen atmosphere.   A typical sample preparation procedure for EXSY experiments is as follows: 19 mg (15 μmol) $[Ni(P^{Cy}_2N^{Bn}_2)_2]^{2+}$ was dissolved in 0.7 mL CD_3CN, making a 20 mM solution.   The solution was purged with H_2 for ~1 minute to quantitatively generate $[Ni(P^{Cy}_2N^{Bn}_2H)_2]^{2+}$, as confirmed by $^{31}P\{^1H\}$ NMR spectroscopy. To this solution, 20 μL of a 0.2 M (4 μmol) *tert*-butylimino-tri(pyrrolidino)phosphorane, BTPP, solution in CD_3CN was added followed by the addition of 15 μL (165 μmol) aniline and 5-50 μL (15-150 μmol) of a 3M H_2O stock solution in CD_3CN or 16-32 μL (880-1700 μmol) pure water.   The sample was allowed to equilibrate at 25 °C for at least 15 minutes before data acquisition.   0.2-0.25 equivalents of the base, BTPP (pK_a = 28.4 for H-BTPP$^+$),[39] were added to samples used for the EXSY kinetic studies in order to increase the concentration of the hydride species.   This was necessary to avoid saturation of magnetization during the exchange processes.   As previously reported, the BTTP and the hydride species alone did not facilitate significant isomerization on the EXSY timescales in the absence of aniline.[18]

For isomer equilibration studies, varying molar equivalents of aniline and/or water were added to a 10 mM solution of $[Ni(P^{Cy}_2N^{Bn}_2)_2]^{2+}$ in CD_3CN at 25 °C. After purging with H_2, as described above, spectra were acquired immediately and again at varying time points for up to 70 hours.

NMR Spectroscopy Experiments. A 300 MHz ^1H frequency Varian VNMRS spectrometer system equipped with a direct detect dual band probe was used for one-dimensional studies. Two-dimensional studies utilized a 500 MHz ^1H frequency Varian VNMRS system with a Varian OneNMR probe. Typical 90° pulses were about 9 μsec for ^1H and about 12 μsec for ^{31}P. $^{31}P\{^1H\}$ NMR spectra were collected with WALTZ ^1H decoupling.   The temperature was controlled using an XRII852 Sample Cooler (FTS Systems, Stone Ridge, NY) FTS chiller system.

The standard phase-sensitive VNMRJ 2D NOESY pulse program with 128-256 increments, 16-64 scans per increment, and 0-100 ms mixing times was used for the $^{31}P\{^1H\}$

EXSY experiments. To minimize the loss of crosspeak intensity due to T_1 relaxation, a maximum of 100 ms mixing times were used for all quantitative experiments. As in previously reported studies of this system, the ^{31}P{^{1}H} EXSY spectra were analyzed using EXSYCalc software (Mestrelab Research) to obtain pseudo first-order rates constants.[18] The EXSYCalc software determines pseudo first-order rate constants for an exchange process based on the relationship between the integrated EXSY crosspeak intensities at a given mixing time to the intensity of the diagonal crosspeaks at a minimal mixing time using the method developed by Perrin.[39] Exchange rates were obtained using a three-site exchange model based on the number of crosspeaks observed in the spectrum for the $\mathbf{ex^{2+}} \leftrightarrows \mathbf{NiH^+}$, $\mathbf{ee^{2+}} \leftrightarrows \mathbf{NiH^+}$, and/or the $\mathbf{ex^{2+}} \leftrightarrows \mathbf{ee^{2+}}$ exchange processes. The pseudo first-order rate constants obtained were then converted to second- or third-order rate constants based on the proposed rate equations which depend on water and/or aniline. For the $\mathbf{ex^{2+}}$ isomer, there are two ^{31}P resonances, where the e/e isomer and the $\mathbf{NiH^+}$ intermediate exhibits only a single resonance. As a result, the rate constants determined by the EXSYcalc fitting process for the $\mathbf{ex^{2+}}$ isomer were then adjusted by a factor of two to compensate for the intensity difference. Each experiment was repeated in triplicate.

Computational details

The structure and thermodynamic properties of each intermediate state and transition state were calculated by using Density Functional Theory with the hybrid B3P86 exchange and correlation functional.[43–45] The Stuttgart basis set with effective core potential was employed for the Ni atom,[46] and 6-31G* for all non-metal atoms with additional p polarization functions on the protic or hydridic hydrogens.[47] This computational protocol has been tested extensively and proved to work well for this class of compounds.[16,22,35,48–51] Harmonic vibrational frequencies were calculated at the optimized structures using the same level of theory to estimate the zero-point energy and thermal contributions ($T = 298$K and $p = 1$ bar) to the gas-phase free energy. In previous studies,[16–18] based on *ab intio* molecular dynamics, we showed explicit solvation must be included to properly describe solvation and desolvation free energies. *Ab intio* molecular dynamics requires a large amount of computer time and CPU allocation, and it is impractical to properly account for all possible reaction possibilities arising in mixed acetonitrile/water solutions. Rather, in this work we resorted to solvation free energies calculated using a mixed cluster/continuum description of the solvent acetonitrile.[52] Specifically, all of the solvent molecules engaging hydrogen bond interactions with the catalyst, water and the base or its

conjugate acid were explicitly included in the calculation. The initial location of these explicit solvent molecules was inferred from force-field based molecular dynamics simulations as described in previous publications.[16,18,51] The rest of the solvent was treated using a self-consistent reaction field model at the same level of theory as for the other steps. The Continuum Polarizable Conductor Model (CPCM) was used with Bondi radii.[53] Customary standard state corrections to solvation energy were applied (see for instance Ref. [52]). Basis set superposition error was accounted using the counterpoise method.[54,55] All of the calculations were performed with Gaussian09.[56]

The activation barriers for the association and dissociation reactions were calculated by performing a scan of the catalysts/substrate distance as discussed in a previous publication.[18] The cost for "pre-organizing" the Ni catalyst for binding with the base or water, which is associated to the accessibility, of the pendant amine (steric hindrance) and the bulkiness of the base or water, indicated as ΔE_{dis} in the text, was estimated from the energy difference between the isolated species at the equilibrium geometry in the hydrogen-bonded complex and the equilibrium geometry when only the solvent is interacting with the protonated amine.[18]

References

1 T. R. Cook, D. K. Dogutan, S. Y. Reece, Y. Surendranath, T. S. Teets and D. G. Nocera, *Chem. Rev.*, 2010, **110**, 6474–6502.

2 H. B. Gray, *Nat. Chem.*, 2009, **1**, 7–7.

3 V. S. Thoi, Y. Sun, J. R. Long and C. J. Chang, *Chem. Soc. Rev.*, 2013, **42**, 2388–2400.

4 R. M. Bullock, *Catalysis without Precious Metals*, Wiley-VCH, Weinheim, 2010.

5 M. Wang, L. Chen and L. Sun, *Energy Environ. Sci.*, 2012, **5**, 6763–6778.

6 P. Du and R. Eisenberg, *Energy Environ. Sci.*, 2012, **5**, 6012–6021.

7 J. R. McKone, S. C. Marinescu, B. S. Brunschwig, J. R. Winkler and H. B. Gray, *Chem. Sci.*, 2014, **5**, 865–878.

8 R. M. Bullock, A. M. Appel and M. L. Helm, *Chem. Commun.*, 2014, **50**, 3125–3143.

9 D. L. DuBois, *Inorg. Chem.*, 2014, **53**, 3935–3960.

10 A. Le Goff, V. Artero, B. Jousselme, P. D. Tran, N. Guillet, R. Metaye, A. Fihri, S. Palacin and M. Fontecave, *Science*, 2009, **326**, 1384–1387.

11 V. Artero, M. Chavarot-Kerlidou and M. Fontecave, *Angew. Chem. Int. Ed.*, 2011, **50**, 7238–7266.

12 T. Liu, D. L. DuBois and R. M. Bullock, *Nat. Chem.*, 2013, **5**, 228–233.

13 M. J. Rose, H. B. Gray and J. R. Winkler, *J. Am. Chem. Soc.*, 2012, **134**, 8310–8313.

14 J. M. Camara and T. B. Rauchfuss, *Nat. Chem.*, 2011, **4**, 26–30.

15 M. L. Singleton, D. J. Crouthers, R. P. Duttweiler, J. H. Reibenspies and M. Y. Darensbourg, *Inorg. Chem.*, 2011, **50**, 5015–5026.

16 S. Raugei, S. Chen, M.-H. Ho, B. Ginovska-Pangovska, R. J. Rousseau, M. Dupuis, D. L. DuBois and R. M. Bullock, *Chem.- Eur. J.*, 2012, **18**, 6493–6506.

17 M. O'Hagan, W. J. Shaw, S. Raugei, S. Chen, J. Y. Yang, U. J. Kilgore, D. L. DuBois and R. M. Bullock, *J. Am. Chem. Soc.*, 2011, **133**, 14301–14312.

18 M. O'Hagan, M.-H. Ho, J. Y. Yang, A. M. Appel, M. R. DuBois, S. Raugei, W. J. Shaw, D. L. DuBois and R. M. Bullock, *J. Am. Chem. Soc.*, 2012, **134**, 19409–19424.

19 J. M. Darmon, S. Raugei, T. Liu, E. B. Hulley, C. J. Weiss, R. M. Bullock and M. L. Helm, *ACS Catal.*, 2014, **4**, 1246–1260.

20 M. L. Helm, M. P. Stewart, R. M. Bullock, M. R. DuBois and D. L. DuBois, *Science*, 2011, **333**, 863–866.

21 M. P. Stewart, M.-H. Ho, S. Wiese, M. L. Lindstrom, C. E. Thogerson, S. Raugei, R. M. Bullock and M. L. Helm, *J. Am. Chem. Soc.*, 2013, **135**, 6033–6046.

22 S. Chen, M.-H. Ho, R. M. Bullock, D. L. DuBois, M. Dupuis, R. Rousseau and S. Raugei, *ACS Catal.*, 2014, **4**, 229–242.

23 P. Das, M.-H. Ho, M. O'Hagan, W. J. Shaw, R. M. Bullock, S. Raugei and M. L. Helm, *Dalton Trans.*, 2014, **43**, 2744–2754.

24 D. H. Pool, M. P. Stewart, M. O'Hagan, W. J. Shaw, J. A. S. Roberts, R. M. Bullock and D. L. DuBois, *Proc. Natl. Acad. Sci.*, 2012, **109**, 15634–15639.

25 J. Y. Yang, S. E. Smith, T. Liu, W. G. Dougherty, W. A. Hoffert, W. S. Kassel, M. R. DuBois, D. L. DuBois and R. M. Bullock, *J. Am. Chem. Soc.*, 2013, **135**, 9700–9712.

26 U. J. Kilgore, J. A. S. Roberts, D. H. Pool, A. M. Appel, M. P. Stewart, M. R. DuBois, W. G. Dougherty, W. S. Kassel, R. M. Bullock and D. L. DuBois, *J. Am. Chem. Soc.*, 2011, **133**, 5861–5872.

27 U. J. Kilgore, M. P. Stewart, M. L. Helm, W. G. Dougherty, W. S. Kassel, M. R. DuBois, D. L. DuBois and R. M. Bullock, *Inorg. Chem.*, 2011, **50**, 10908–10918.

28 T. Liu, S. Chen, M. J. O'Hagan, M. Rakowski DuBois, R. M. Bullock and D. L. DuBois, *J. Am. Chem. Soc.*, 2012, **134**, 6257–6272.

29 S. Hammes-Schiffer, *Acc. Chem. Res.*, 2009, **42**, 1881–1889.

30 D. R. Weinberg, C. J. Gagliardi, J. F. Hull, C. F. Murphy, C. A. Kent, B. C. Westlake, A. Paul, D. H. Ess, D. G. McCafferty and T. J. Meyer, *Chem. Rev.*, 2012, **112**, 4016–4093.

31 M. H. V. Huynh and T. J. Meyer, *Chem. Rev.*, 2007, **107**, 5004–5064.

32 A. D. Wilson, R. K. Shoemaker, A. Miedaner, J. T. Muckerman, D. L. DuBois and M. R. DuBois, *Proc. Natl. Acad. Sci.*, 2007, **104**, 6951–6956.

33 G. M. Jacobsen, R. K. Shoemaker, M. J. McNevin, M. Rakowski DuBois and D. L. DuBois, *Organometallics*, 2007, **26**, 5003–5009.

34 R. M. Henry, R. K. Shoemaker, D. L. DuBois and M. R. DuBois, *J. Am. Chem. Soc.*, 2006, **128**, 3002–3010.

35 M.-H. Ho, S. Chen, R. Rousseau, M. Dupuis, R. M. Bullock and S. Raugei, in *Applications of Molecular Modeling to Challenges in Clean Energy*, eds. G. Fitzgerald and N. Govind, American Chemical Society, Washington, DC, 2013, vol. 1133, pp. 89–111.

36 J. Hou, M. Fang, A. J. P. Cardenas, W. J. Shaw, M. L. Helm, R. M. Bullock, J. A. S. Roberts and M. O'Hagan, *Energy Environ. Sci.*, 2014, **7**, 4013–4017.

37 W. A. Hoffert, J. A. S. Roberts, R. M. Bullock and M. L. Helm, *Chem. Commun.*, 2013, **49**, 7767–7769.

38 J. Y. Yang, R. M. Bullock, W. J. Shaw, B. Twamley, K. Fraze, M. R. DuBois and D. L. DuBois, *J. Am. Chem. Soc.*, 2009, **131**, 5935–5945.

39 I. Kaljurand, A. Kütt, L. Soovali, T. Rodima, V. Mäemets, I. Leito and I. A. Koppel, *J. Org. Chem.*, 2005, **70**, 1019–1028.

40 A. E. Reed, L. A. Curtiss and F. Weinhold, *Chem. Rev.*, 1988, **88**, 899–926.

41 M. K. Chantooni Jr and I. M. Kolthoff, *J. Am. Chem. Soc.*, 1970, **92**, 2236–2239.

42 A. M. Appel, D. H. Pool, M. O'Hagan, W. J. Shaw, J. Y. Yang, M. Rakowski DuBois, D. L. DuBois and R. M. Bullock, *ACS Catal.*, 2011, **1**, 777–785.

43 J. P. Perdew, *Phys. Rev. B*, 1986, **34**, 7406–7406.

44 J. P. Perdew, *Phys. Rev. B*, 1986, **33**, 8822–8824.

45 A. D. Becke, *Phys. Rev. A*, 1988, **38**, 3098–3100.

46 D. Andrae, U. Häußermann, M. Dolg, H. Stoll and H. Preuß, *Theor. Chim. Acta*, 1990, **77**, 123–141.

47 V. A. Rassolov, J. A. Pople, M. A. Ratner and T. L. Windus, *J. Chem. Phys.*, 1998, **109**, 1223.

48 S. Chen, S. Raugei, R. Rousseau, M. Dupuis and R. M. Bullock, *J. Phys. Chem. A*, 2010, **114**, 12716–12724.

49 S. Chen, R. Rousseau, S. Raugei, M. Dupuis, D. L. DuBois and R. M. Bullock, *Organometallics*, 2011, **30**, 6108–6118.

50 M. Dupuis, S. Chen, S. Raugei, D. L. DuBois and R. M. Bullock, *J. Phys. Chem. A*, 2011, **115**, 4861–4865.

51 M.-H. Ho, S. Raugei, R. Rousseau, M. Dupuis and R. M. Bullock, *J. Chem. Theory Comput.*, 2013, **9**, 3505–3514.

52 V. S. Bryantsev, M. S. Diallo and W. A. Goddard III, *J. Phys. Chem. B*, 2008, **112**, 9709–9719.

53   A. Bondi, *J. Phys. Chem.*, 1964, **68**, 441–451.

54   S. F. Boys and F. Bernardi, *Mol. Phys.*, 1970, **19**, 553–557.

55   S. Simon, M. Duran and J. J. Dannenberg, *J. Chem. Phys.*, 1996, **105**, 11024–11031.

56   M. J. Frisch, G. W. Trucks, H. B. Schlegel, G. E. Scuseria, M. A. Robb, J. R. Cheeseman, G. Scalmani, V. Barone, B. Mennucci, G. A. Petersson, H. Nakatsuji, M. Caricato, X. Li, H. P. Hratchian, A. F. Izmaylov, J. Bloino, G. Zheng, J. L. Sonnenberg, M. Hada, M. Ehara, K. Toyota, R. Fukuda, J. Hasegawa, M. Ishida, T. Nakajima, Y. Honda, O. Kitao, H. Nakai, T. Vreven, J. A. Montgomery, Jr., J. E. Peralta, F. Ogliaro, M. Bearpark, J. J. Heyd, E. Brothers, K. N. Kudin, V. N. Staroverov, R. Kobayashi, J. Normand, K. Raghavachari, A. Rendell, J. C. Burant, S. S. Iyengar, J. Tomasi, M. Cossi, N. Rega, N. J. Millam, M. Klene, J. E. Knox, J. B. Cross, V. Bakken, C. Adamo, J. Jaramillo, R. Gomperts, R. E. Stratmann, O. Yazyev, A. J. Austin, R. Cammi, C. Pomelli, J. W. Ochterski, R. L. Martin, K. Morokuma, V. G. Zakrzewski, G. A. Voth, P. Salvador, J. J. Dannenberg, S. Dapprich, A. D. Daniels, O. Farkas, J. B. Foresman, J. V. Ortiz, J. Cioslowski and D. J. Fox, *Gaussian 09, Revision A.1*, Gaussian, Inc., Wallingford, CT, 2009.